Microstructures and Mechanical Properties of Welded Fe-12Cr-20Mn Austenitic Stainless Steel

I.J. Eldridge and D.J. Morrison

The effects of welding on the tensile and fatigue properties of fully annealed and cold-worked Fe-12Cr-20Mn austenitic stainless steel were evaluated. Room temperature and 500 °C tensile tests and room temperature cantilever beam fatigue tests were accomplished on specimens that contained autogenous bead-on-plate welds. The tensile and fatigue properties of the fully annealed material were not significantly influenced by welding. The tensile properties of the welded cold-worked material were also not significantly affected by the presence of a weldment. However, welding caused a large reduction of the fatigue life of the cold-worked material. Fatigue cracks preferentially initiated at large Mn-Si inclusions that formed in the fusion zones of the weldments.

Keywords
austenitic steels, fatigue, fusion energy, tensile properties, welding

1. Introduction

ONE of the more difficult challenges facing designers of nuclear fusion reactors is the selection of a first-wall material that will withstand the severe thermal and radiation environment. In addition to these performance criteria, the material must exhibit rapid decay of induced radioactivity to minimize structural material disposal problems when the reactor is decommissioned. As a result, extensive research is being conducted on the development of fast induced radioactivity decay (FIRD) materials for use in fusion reactors (Ref 1). In these materials, the levels of Ni, Mo, Nb, N, and Cu must be minimized or preferably eliminated (Ref 2-4). The restrictions on Ni and Mo are especially significant because they are critical alloying elements in steels currently used in nuclear fission reactors.

One approach to the development of FIRD austenitic stainless steels is to replace Ni with Mn (Ref 4-10). Klueh and Maziasz (Ref 4) performed extensive studies on Fe-Cr-Mn alloys and concluded that an alloy of Fe-12% Cr-20% Mn-0.25% C would be ideal for austenite stability and would exhibit similar or superior mechanical properties to AISI 316 stainless steel (Ref 4, 11). Ferritic FIRD steels were proposed that replace Mo with varying amounts of W and V (Ref 12, 13).

The weldability of fusion reactor materials is a very important consideration. Fission reactors can be designed with weldments outside the regions of most intense radiation, temperature, and mechanical stress. However, this is not possible in the design of fusion reactors (Ref 14). The effects of welding are especially important in light of the fact that reactor structures are often fabricated with metal in a cold-worked condition to optimize resistance to radiation effects. Clearly this advantage would be lost in the vicinity of a weldment. In response to this need for an understanding of the effects of welding on the mechanical behavior of potential fusion reactor materials, this research study was initiated to evaluate the effects of a weldment on the tensile and fatigue properties of a FIRD Fe-Cr-Mn alloy.

I.J. Eldridge and **D.J. Morrison,** Department of Mechanical and Aeronautical Engineering, Clarkson University, Potsdam, NY 13699-5729, USA

2. Experimental Procedures

A vacuum induction melting process was used to produce an ingot with composition 12.12 wt.% Cr, 20.16 wt.% Mn, 0.23 wt.% C, 0.29 wt.% Si, and balance Fe. The ingot was hot-rolled to a thickness of 3.17 mm and pickled. The slab was then cold rolled to a thickness of 2.54 mm (20% cold worked) and sheared in half. One half was then cold rolled to a final thickness of 1.27 mm (60% cold worked). The 60% cold-worked metal was annealed at 1100 °C for 45 min and water quenched. This material is referred to as FA (fully annealed). The slab cold rolled to a thickness of 2.54 mm is referred to as CW (cold worked).

Autogenous bead-on-plate gas tungsten arc (GTA) welds were made on the FA and CW plates according to the parameters shown in Table 1. The arc length (distance from the torch tip to the workpiece) was 3.2 mm, and the polarity was dc electrode negative. Tensile specimens were milled from the welded plates as scaled versions of the ASTM E-8 standard pin-loaded tensile specimen with the longitudinal (tensile) axis of the specimen parallel to the rolling direction of the base metal. Welds were located in the center of the gage section and oriented perpendicular to the tensile axis. For comparison purposes, several tensile specimens were made without welds. Tensile tests were accomplished at room temperature using an Applied Test Systems, Inc., Butler, PA, universal testing machine and at 500 °C on a Duffers Gleeble 510, Duffers Scientific, Inc., Poestenkill, NY, hot ductility testing machine.

Cantilever beam fatigue specimens were milled from the welded FA and CW plates with the long axis of the specimen parallel to the rolling direction. The specimens were designed with a tapered gage section to produce a region of constant sur-

Table 1 Welding parameters

Specimen type	Electrode diameter, mm	Travel speed, mm/min	Argon flow rate, m^3/h	Current, amperes
Fe-Cr-Mn FA	3.175	444.5	0.283	60
Fe-Cr-Mn CW	3.175	444.5	0.283	80

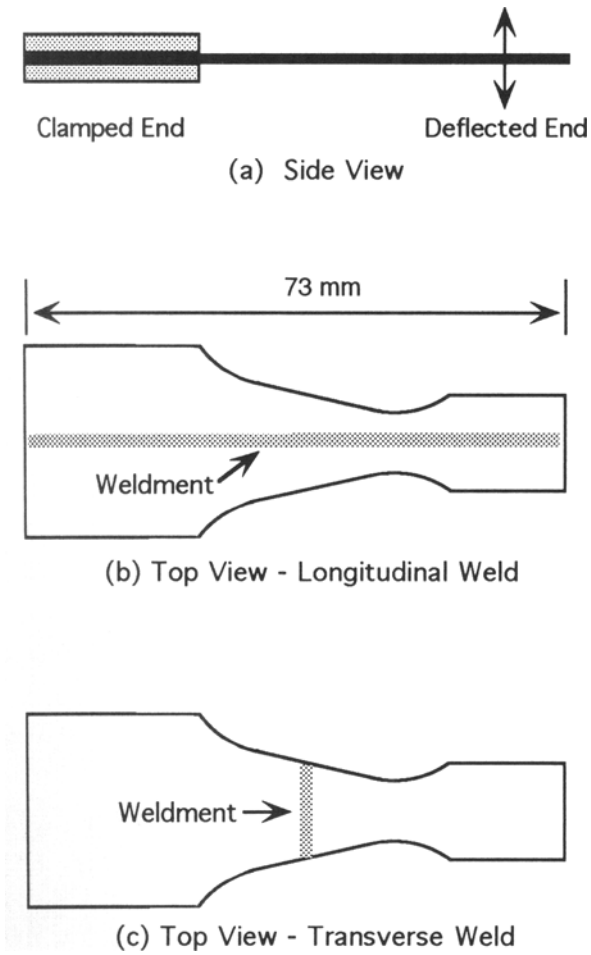

Fig. 1 Cantilever beam fatigue specimen geometry

face stress. Specimens were produced with welds oriented in the longitudinal and transverse directions as shown in Fig. 1. The specimens were ground to a thickness of 1 mm using SiC paper and electropolished in a solution of 350 mL ethanol, 60 mL H_2O, 50 mL butoxyethanol, and 40 mL perchloric acid at a temperature of –30 °C and potential of 40 volts. The fatigue tests were accomplished at a cycling rate of 25 Hz, and the deflection of the fatigue apparatus was set to produce a fully reversed total strain amplitude, ε_t, of 0.25% at the surface of the gage section. In addition, one FA specimen was tested at ε_t = 0.50% and cycling rate of 3.5 Hz. Fatigue failure was defined as the point when the peak bending moment decreased 20% from the value at the beginning of the test. During the tests, acetate surface replicas were obtained to provide a record of the evolution of fatigue damage.

Coupons of weld regions for microstructural analyses were prepared using standard metallographic procedures and electropolished with the same electrolyte mentioned above. Etching was performed with either Beraha's tint etchant (Ref 15) or a grain boundary etchant consisting of equal parts of HCl, HNO_3, and H_2O. Microstructural studies of the base and weld metals were performed using optical and scanning electron microscopy and X-ray energy dispersive spectroscopy (EDS). Microhardness traverses across the weld sections were obtained using a Leco M-400, LecoCorp., St. Joseph, MI, micro-

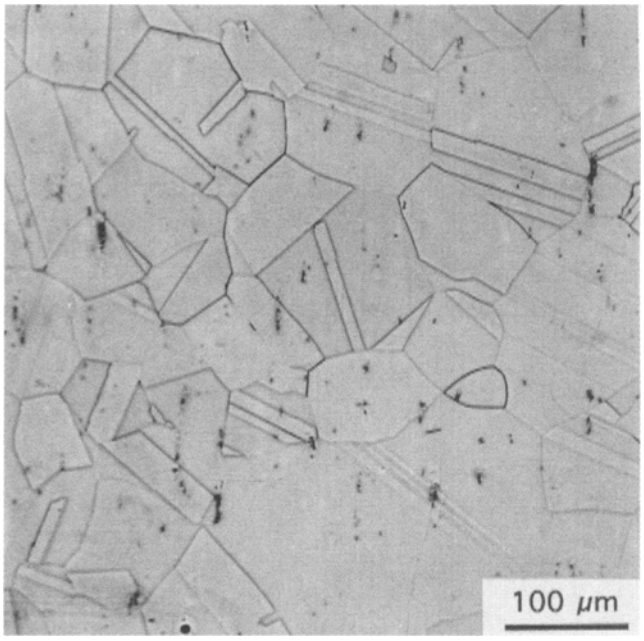

Fig. 2 Optical micrograph of FA base metal with the grain boundary etchant

hardness tester with a Vickers indenter and 30 g load. A Fischer MP3 Feritescope, Fischer Technology, Inc., Windsor, CT, was used to determine ferrite numbers of the various regions of the specimens. The ferrite numbers provided an estimate of the relative amounts of ferrite and austenite in the microstructures (Ref 16).

3. Results and Discussion

Micrographs shown in Fig. 2 and 3 depict the base metal and fusion zone (metal that melted and resolidified) of the FA specimen. Ferrite numbers of the base metal and fusion zone were zero, which indicated that the microstructures were almost completely austenitic. As shown in Fig. 2, the base metal consists of austenite grains, annealing twins, and inclusions. The inclusions appear to form clusters that are elongated in the rolling direction, which runs from the bottom of the micrograph to the top. EDS analysis of the inclusions indicated that they are primarily composed of manganese and silicon. Figure 3 shows that the fusion zone consists of a dendritically-cored structure with very small precipitates. The FA specimen did not exhibit a distinct heat affected zone (HAZ). The fusion zone of the CW specimen was identical to that of the FA specimen. The HAZ of the CW specimen was nearly identical to the FA base metal.

Graphs shown in Fig. 4 and 5 depict the variations of microhardness across the weldments in the FA and CW specimens. The slight increase in hardness of the FA fusion zone is the result of the smaller grains produced during the welding. As expected, welding caused a significant decrease in hardness of the HAZ and fusion zone of the CW specimen.

The results of tensile tests of welded and unwelded specimens accomplished at room temperature and 500 °C are shown in Table 2. The FA welded specimens tested at room temperature all fractured in the base metal whereas the specimen tested

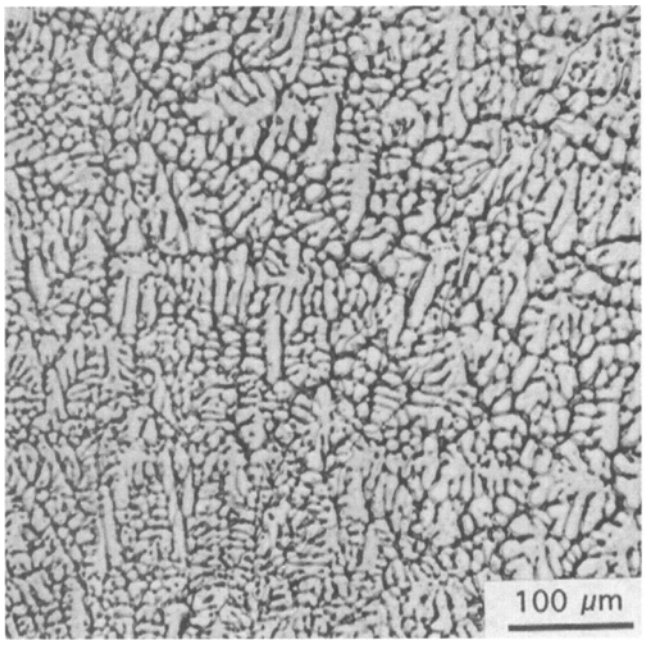

Fig. 3 Optical micrograph of the fusion zone of a FA specimen etched with Beraha's etchant

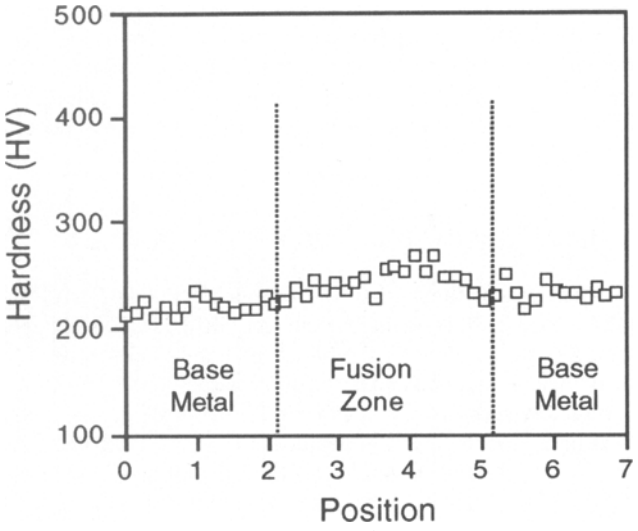

Fig. 4 Microhardness traverse across the base metal and fusion zone of the FA specimen

at 500 °C fractured at the interface between the base metal and fusion zone. The CW welded specimens tested at room temperature all fractured in the fusion zone. The values listed in Table 2 indicate that the presence of the weldment did not significantly affect tensile strength or ductility. Even though the weldment in the CW specimen was significantly softer than the base metal, the presence of the weldment lowered the tensile strength only slightly. Because this alloy in the annealed condition has a very high strain hardening capacity, the soft weld region experienced considerable strain hardening and resulted in only a small reduction of tensile strength. While the presence of a weldment did not significantly affect tensile

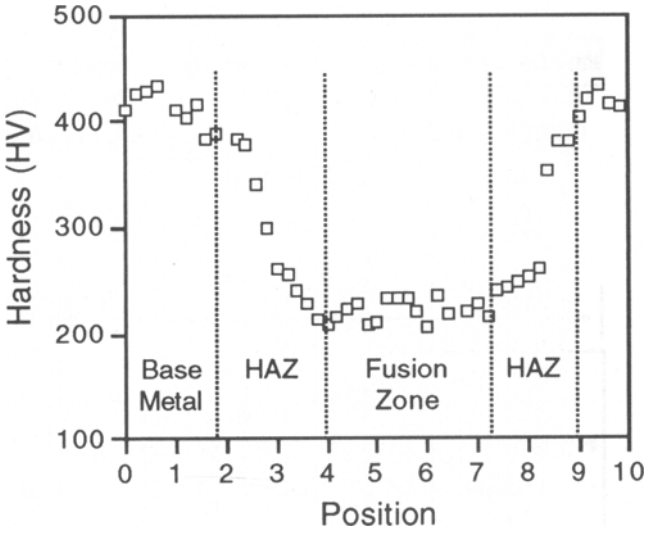

Fig. 5 Microhardness traverse across the base metal, HAZ, and fusion zone of the CW specimen

Table 2 Tensile test results

Speciment	Temperature, °C	σ_{yield}, MPa	σ_{uts}, MPa	Elongation, %
FA unwelded	21	292	778	88.5
FA welded	21	272	821	71.4
FA unwelded	500	...	256	42.2
FA welded	500	...	264	40.5
CW unwelded	21	430	1139	31.3
CW welded	21	...	974	25.0

properties, elevated temperature caused a large reduction of tensile strength and ductility.

The room temperature tensile properties are reasonably close to those reported previously for similar unwelded Fe-Cr-Mn alloys (Ref 9, 10). However, Fenici and Scheurer (Ref 6) reported tensile strengths of approximately 410 MPa at 550 °C and 480 at 450 °C compared to 256 MPa at 500 °C in the present study.

Results of the fatigue tests indicated that the weldments were not detrimental to the fatigue resistance of the FA alloy but significantly reduced the fatigue life of the CW alloy. When cycled at ε_t = 0.25%, the FA specimen with longitudinal weld failed after 210 000 cycles, and the FA specimen with transverse weld failed after 200 000 cycles. An unwelded FA specimen cycled at the same strain amplitude failed after 180 000 cycles. Micrographs shown in Fig. 6 and 7 depict the base metal and fusion zone of a FA specimen with longitudinal weld that was fatigued for 210 000 cycles at ε_t = 0.25%. Numerous cracks were observed in both the base metal and fusion zone. The cracks propagated along slip bands and grain boundaries. Replicas indicated that the fatal crack initiated in the base metal near the fusion zone.

The presence of weldments significantly reduced the fatigue lives of the CW specimens. At ε_t = 0.25%, the CW unwelded specimen failed after 1 034 000 cycles. At the same strain amplitude, the CW specimen with longitudinal weld

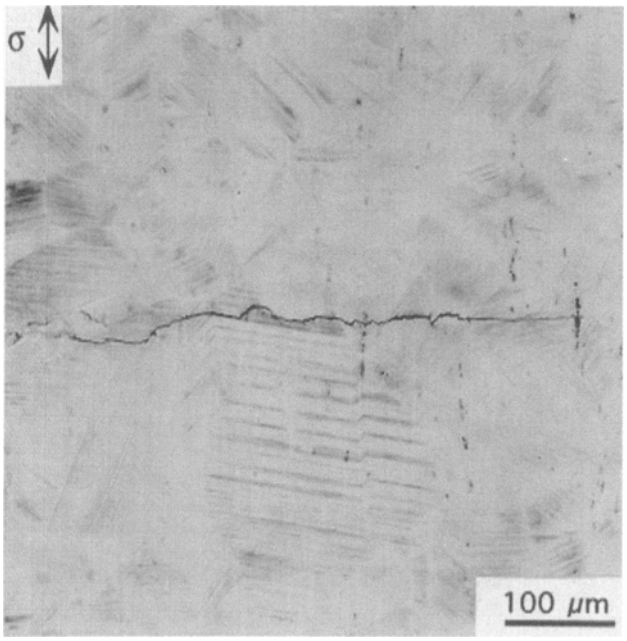

Fig. 6 Optical micrograph of the base metal of the FA specimen with longitudinal weld cycled for 210 000 cycles at $\varepsilon_t = 0.25\%$

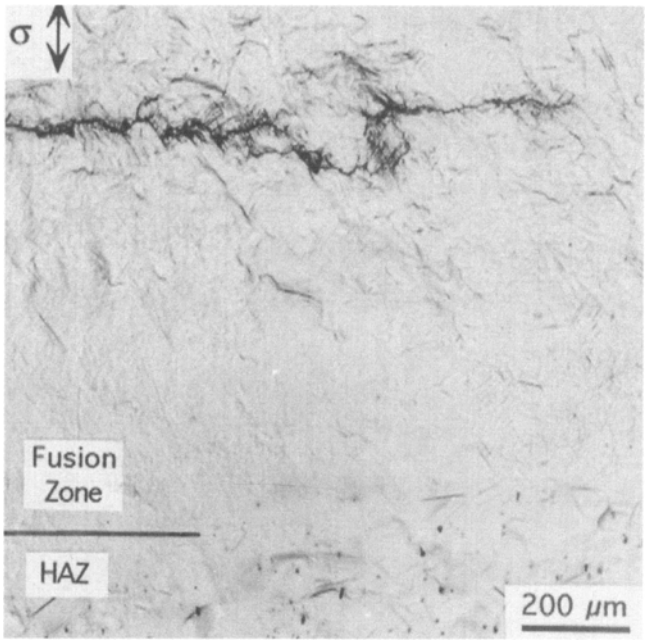

Fig. 7 Optical micrograph of the fusion zone of the FA specimen with longitudinal weld cycled for 210 000 cycles at $\varepsilon_t = 0.25\%$

failed after 373 000 cycles, and the CW specimen with transverse weld failed after 182 000 cycles. In the CW specimen with longitudinal weld, even though the total strain amplitude was the same in the base metal and weld zone, the lower yield strength of the soft weld zone caused the plastic strain to be greater in that area, thus accounting for the reduction of fatigue life. Numerous fatigue cracks were observed in the HAZ and fusion zone of this specimen. However, no fatigue damage was

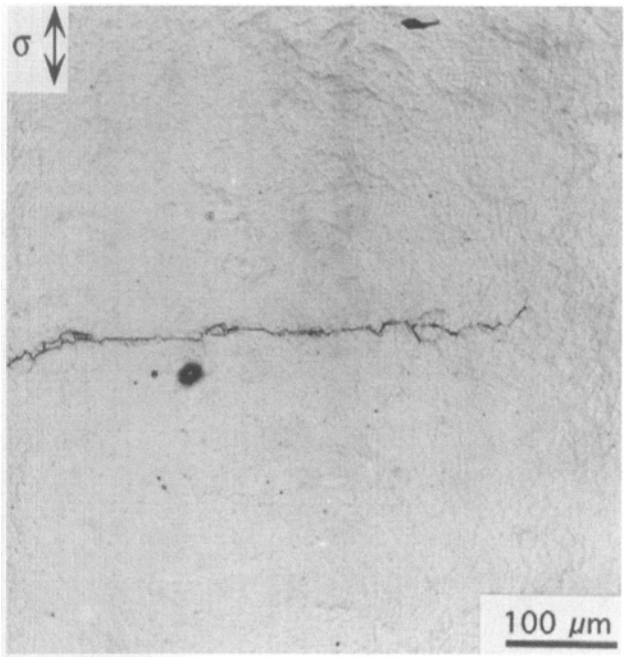

Fig. 8 Optical micrograph showing the fatigue crack in the fusion zone of the CW specimen with transverse weld. This specimen was cycled for 182 000 cycles at $\varepsilon_t = 0.25\%$

detected in the base metal. In the CW specimen with transverse weld, the soft weld zone formed a plastic hinge, which concentrated strain in the weld zone and caused a significant reduction of fatigue life. Figure 8 shows extensive fatigue damage in the fusion zone of the CW specimen with transverse weld after 182 000 cycles.

One FA specimen with longitudinal weld was cycled at $\varepsilon_t = 0.50\%$. This specimen failed after 20 000 cycles. The surface of the base metal was almost completely covered with intense slip bands. Numerous fatigue cracks were also present in the base metal. Slip bands were much less pronounced in the fusion zone, but many fatigue cracks were present. Figure 9 depicts a crack that extended from the base metal into the fusion zone. As shown in Fig. 10, fusion zone fatigue cracks were frequently aligned with the columnar grain structure of the fusion zone. Near the base metal, fusion zone cracks were oriented about 60 degrees to the longitudinal stress direction. These cracks are identified with "a" in Fig. 10. In the center of the fusion zone, a more equiaxed grain structure was produced. As a result, the cracks were oriented perpendicular to the stress direction as shown by the crack identified by "b" in Fig. 10. Replicas indicated that cracks initiated in both the fusion zone and base metal.

Very large spherical inclusions with diameters approaching 40 μm were observed in the fusion zones and most frequently at the edge of the fusion zone near the HAZ (CW specimens) or base metal (FA specimens). Fatigue cracks frequently initiated at these inclusions. The replica micrograph of Fig. 11 depicts a large inclusion in the FA specimen with longitudinal weld, which was cycled for 40 000 cycles at $\varepsilon_t = 0.25\%$. A short crack to the left of the inclusion is identified by the arrow. The same inclusion after 300 000 cycles is shown in the replica micrograph of Fig. 12 where cracks are seen extending from both sides of the inclusion. Another inclusion is shown in the scanning electron micrograph of Fig. 13, which was obtained from

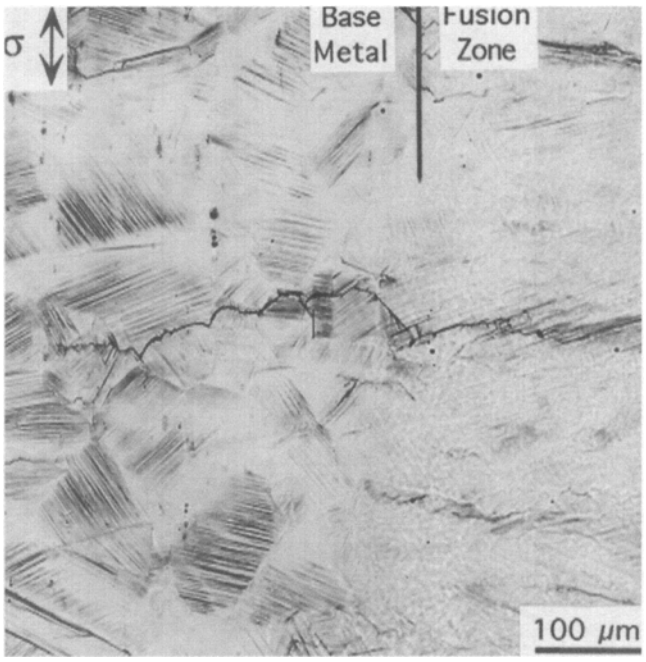

Fig. 9 Optical micrograph of the FA specimen with longitudinal weld cycled for 20 000 cycles at $\varepsilon_t = 0.50\%$

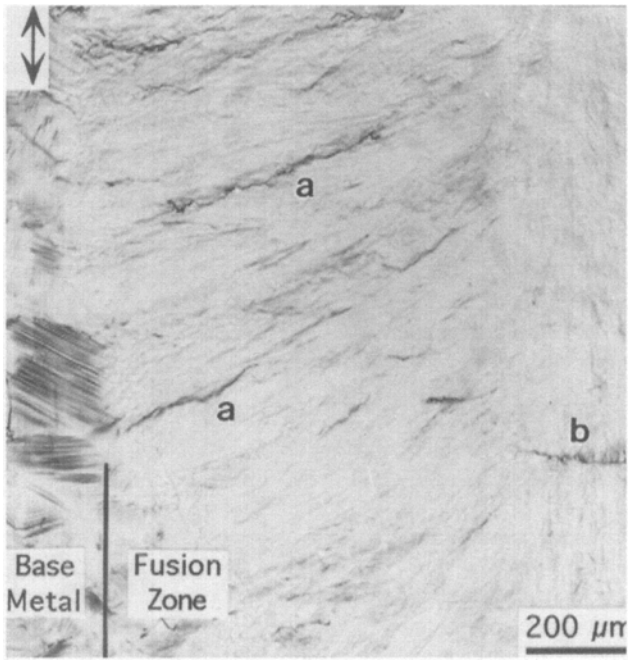

Fig. 10 Optical micrograph of the FA specimen with longitudinal weld cycled for 20 000 cycles at $\varepsilon_t = 0.50\%$ showing the alignment of cracks in the fusion zone. The letter "a" identifies cracks aligned with the columnar solidification structure, and "b" shows the orientation of a crack in the central equiaxed region of the fusion zone

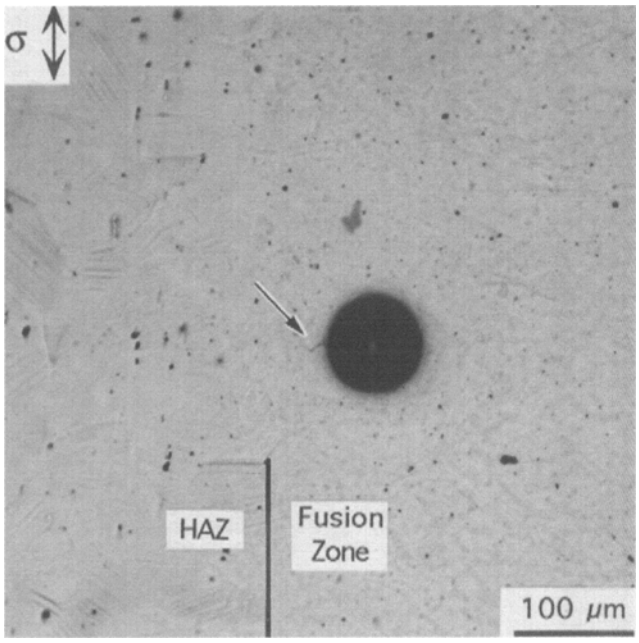

Fig. 11 Optical micrograph of a replica of the CW specimen with longitudinal weld cycled at $\varepsilon_t = 0.25\%$. The replica was obtained after 40 000 fatigue cycles. A small crack (identified by the arrow) extends from the left of the inclusion

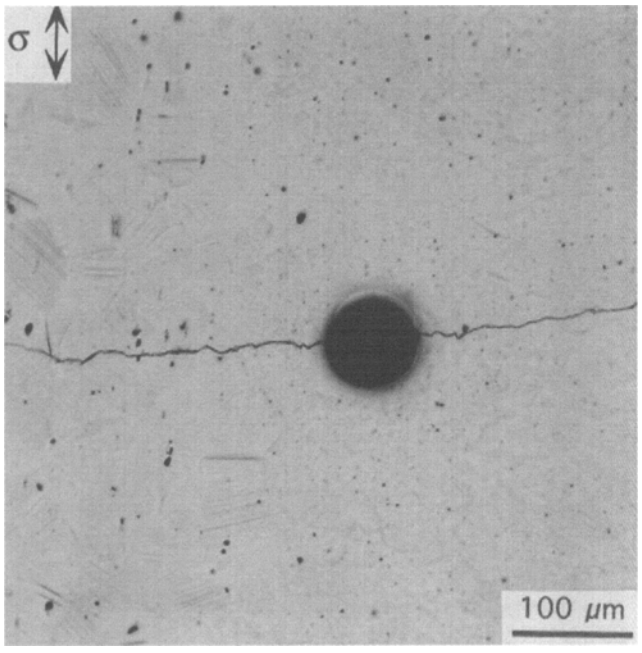

Fig. 12 Optical micrograph of a replica depicting the same area as Fig. 11. This replica was obtained after 300 000 fatigue cycles

the FA specimen with longitudinal weld, which was cycled for 20 000 cycles at $\varepsilon_t = 0.50\%$. The fatigue crack extends completely through the inclusion. An EDS analysis of this inclusion indicated that its composition was similar to the small inclusions in the base metal discussed previously, i.e. composed of manganese and silicon. Large inclusions were probably present in the original ingot of the alloy. Hot and cold rolling broke the inclusions into much smaller particles and aligned them in the rolling direction to form stringers or elongated clusters. Examples of these elongated clusters are shown in the base metals in Fig. 2, 6, and 9. The small inclusions did not appear to be af-

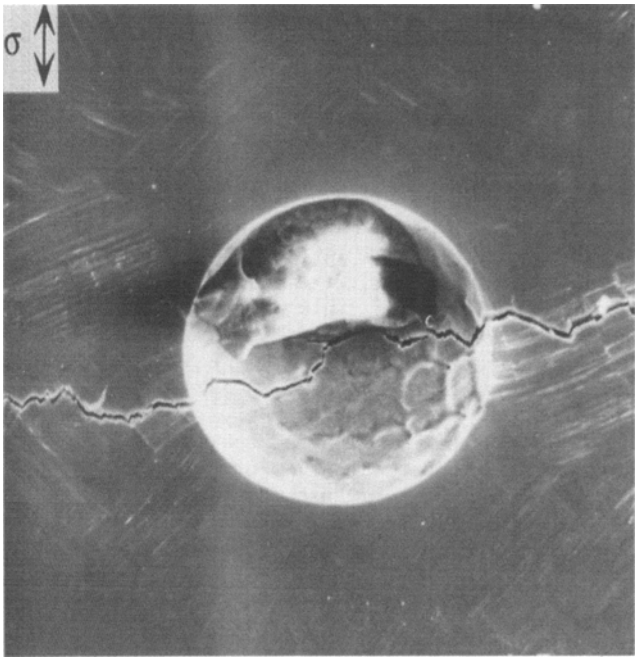

Fig. 13 Scanning electron micrograph of an inclusion in the FA specimen with longitudinal weld cycled for 20 000 cycles at ε_t = 0.50%

fected by the annealing heat treatment. However, during welding, the inclusions probably dissolved in the molten metal and reformed as large inclusions upon subsequent solidification of the weld metal.

4. Conclusion

From the results of this research, the following conclusions are made concerning the microstructures and mechanical properties of welded Fe-12Cr-20Mn stainless steel:

- Autogenous welding of Fe-12Cr-20Mn produced a dendritically cored austenitic microstructure.
- The presence of a weldment did not appreciably affect the room temperature tensile strengths of Fe-12Cr-20Mn in the FA and CW conditions.
- Elevated temperature (500 °C) caused a large reduction of tensile strength. However, the presence of a weldment did not degrade tensile properties at 500 °C.
- Fatigue properties of the FA alloy were not significantly affected by welding.
- The presence of a weldment accelerated fatigue failure in the CW alloy.
- Large inclusions formed in the fusion zone of the Fe-12Cr-20Mn alloy. These inclusions consisted primarily of Mn and Si. Fatigue cracks initiated at these inclusions.

Acknowledgments

This material is based on work supported by the National Science Foundation under grant 9108695.

References

1. R.L. Klueh, Developing Steels for Service in Fusion Reactors, *J. Met.*, Vol 44 (No. 4), 1992, p 20-24
2. D.S. Gelles, Effects of Irradiation on Low Activation Ferritic Alloys: A Review, *Reduced Activation Materials for Fusion Reactors—ASTM STP 1047*, R.L. Klueh, D.S. Gelles, M. Okada, and N.H. Packan, Ed., American Society for Testing and Materials, 1990, p 113-129
3. M. Okada, T. Noda, and F. Abe, On the Development of Low-Activation Materials for Fusion Reactors, *J. Nucl. Mater.*, Vol 169, 1989, p 249-256
4. R.L. Klueh and P.J. Maziasz, Reduced Activation Austenitic Stainless Steels: The Fe-Mn-Cr-C System, *Reduced Activation Materials for Fusion Reactors—ASTM STP 1047*, R.L. Klueh, D.S. Gelles, M. Okada, and N.H. Packan, Ed., American Society for Testing and Materials, 1990, p 7-18
5. H. Yoshida, K. Miyata, H. Kodaka, and S. Nishikawa, Irradiation Effects on Mechanical Properties of High Manganese Steels, *Reduced Activation Materials for Fusion Reactors—ASTM STP 1047*, R.L. Klueh, D.S. Gelles, M. Okada, and N.H. Packan, Ed., American Society for Testing and Materials, 1990, p 47-55
6. P. Fenici and H. Scheurer, Tensile Properties of Neutron Irradiated Cr-Mn Austenitic Stainless Steels, *J. Nucl. Mater.*, Vol 155-157, 1988, p 947-952
7. F.A. Garner, F. Abe, and T. Noda, Response of Fe-Cr-Mn Austenitic Alloys to Thermal Aging and Neutron Irradiation, *J. Nucl. Mater.*, Vol 155-157, 1988, p 870-876
8. J.M. McCarthy and F.A. Garner, Phase Instabilities in Irradiated Simple Fe-Cr-Mn Low Activation Alloys, *J. Nucl. Mater.*, Vol 155-157, 1988, p 877-882
9. K. Miyahara, Y. Okazaki, M. Mochizuki, Y. Hosoi, and H. Kayano, Mechanical Properties and Microstructure of α-Particle Irradiated Fe-12%Cr-15,30% Mn Alloys, *J. Nucl. Mater.*, Vol 155-157, 1988, p 1054-1058
10. A.V. Vertkov, V.A. Evtikhin, I.E. Lyublinski, A.A. Syichev, E.V. Demina, and M.D. Prusakova, Mechanical Properties of Low-Activation Cr-Mn Austenitic Steels Changes in Liquid Lithium, *J. Nucl. Mater.*, Vol 203, 1993, p 158-163
11. P.J. Maziasz and R.L. Klueh, Precipitation Sensitivity to Alloy Composition in Fe-Cr-Mn Austenitic Steels Developed for Reduced Activation for Fusion Application, *Reduced Activation Materials for Fusion Reactors—ASTM STP 1047*, R.L. Klueh, D.S. Gelles, M. Okada, and N.H. Packan, Ed., American Society for Testing and Materials, 1990, p 56-79
12. R.P. Klueh and P.J. Maziasz, The Microstructure of Chromium-Tungsten Steels, *Metall. Trans. A*, Vol 20, 1989, p 373-382
13. R.L. Klueh, Irradiation Hardening of Ferritic Steels: Effect of Composition, *J. Nucl. Mater.*, Vol 179-181, 1991, p 728-732
14. H. Ullmaier, Fusion Materials Research: Problems—Recent Developments—Present Trends, *Fusion Eng. Des.*, Vol 14, 1991, p 155-160
15. G.F. Vander Voort, *Metallography: Principles and Practice*, McGraw-Hill Book Company, 1984, p 653 (etchant 196)
16. J.A. Brooks and J.C. Lippold, Selection of Wrought Austenitic Stainless Steel, *Metals Handbook*, Vol 6, ASM International, 1993, p 461